

RESEARCH ARTICLE | MARCH 20 2023

## Multi-angle *in situ* dynamic light scattering at a neutron spin echo spectrometer

F. Vögl; L. Balacescu; O. Holderer; ... et. al



Rev Sci Instrum 94, 034106 (2023)

<https://doi.org/10.1063/5.0136367>



View  
Online



Export  
Citation

CrossMark

### Articles You May Be Interested In

The role of hydrophobicity in the cold denaturation of proteins under high pressure: A study on apomyoglobin

*J. Chem. Phys.* (February 2019)

Energy and volume changes induced by photoinitiated proton releasing reaction with apomyoglobin

*Rev Sci Instrum* (January 2003)

Nonphotochemical holeburning in a protein matrix: Chlorophyllide in apomyoglobin

*J. Chem. Phys.* (February 1987)



Time to get excited.  
Lock-in Amplifiers – from DC to 8.5 GHz

[Find out more](#)

 Zurich  
Instruments

# Multi-angle *in situ* dynamic light scattering at a neutron spin echo spectrometer

Cite as: Rev. Sci. Instrum. 94, 034106 (2023); doi: 10.1063/5.0136367

Submitted: 25 November 2022 • Accepted: 23 February 2023 •

Published Online: 20 March 2023



View Online



Export Citation



CrossMark

F. Vögl,<sup>1,2</sup>  L. Balacescu,<sup>1,3</sup>  O. Holderer,<sup>1</sup>  S. Pasini,<sup>1</sup>  S. Staringer,<sup>1</sup> G. Brandl,<sup>1</sup>  V. Ossovyi,<sup>1</sup>  
H. Feilbach,<sup>4</sup> P. Müller-Buschbaum,<sup>2,5</sup>  A. M. Stadler,<sup>4,6</sup>  J. Fitter,<sup>3,7</sup>  and T. E. Schrader<sup>1,a)</sup> 

## AFFILIATIONS

<sup>1</sup>Forschungszentrum Jülich GmbH, Jülich Centre for Neutron Science (JCNS) at Heinz Maier-Leibnitz Zentrum (MLZ), 85748 Garching, Germany

<sup>2</sup>Technical University of Munich, TUM School of Natural Sciences, Department of Physics, Chair for Functional Materials, James-Franck-Str. 1, 85748 Garching, Germany

<sup>3</sup>RWTH Aachen, Physikalisches Institut (IA), AG Biophysik, 52074 Aachen, Germany

<sup>4</sup>Forschungszentrum Jülich GmbH, Jülich Centre for Neutron Science (JCNS-1) and Institute of Biological Information Processing (IBI-8), 52425 Jülich, Germany

<sup>5</sup>Technische Universität München, MLZ, Lichtenbergstr. 1, 85748 Garching, Germany

<sup>6</sup>RWTH Aachen University, Institute of Physical Chemistry, Landoltweg 2, 52056 Aachen, Germany

<sup>7</sup>Forschungszentrum Jülich GmbH, Institute of Biological Information Processing (IBI-6), 52425 Jülich, Germany

<sup>a)</sup> Author to whom correspondence should be addressed: [t.schrader@fz-juelich.de](mailto:t.schrader@fz-juelich.de)

## ABSTRACT

A new sample environment, called Bio-Oven, has been built for the Neutron Spin Echo (NSE) Spectrometer J-NSE Phoenix. It provides active temperature control and the possibility to perform Dynamic Light Scattering (DLS) measurements during the neutron measurement. DLS provides diffusion coefficients of the dissolved nanoparticles, and thus one can monitor the aggregation state of the sample on a time scale of minutes during the spin echo measurement times on the order of days. This approach helps to validate the NSE data or to replace the sample when its aggregation state influences the spin echo measurement results. The new Bio-Oven is an *in situ* DLS setup based on optical fibers decoupling the free space optics around the sample cuvette in a lightproof casing from the laser sources and the detectors. It collects light from three scattering angles simultaneously. Six different values of momentum transfer can be accessed by switching between two different laser colors. Test experiments were performed with silica nanoparticles with diameters ranging from 20 nm up to 300 nm. Their hydrodynamic radii were determined from DLS measurements and compared with the ones obtained by a commercial particle sizer. It was demonstrated that also the static light scattering signal can be processed and gives meaningful results. The protein sample apomyoglobin was used for a long-term test and in a first neutron measurement using the new Bio-Oven. The results prove that the aggregation state of the sample can be followed using *in situ* DLS along with the neutron measurement.

© 2023 Author(s). All article content, except where otherwise noted, is licensed under a Creative Commons Attribution (CC BY) license (<http://creativecommons.org/licenses/by/4.0/>). <https://doi.org/10.1063/5.0136367>

## I. INTRODUCTION

Neutron Spin Echo Spectroscopy (NSE) has the highest energy resolution (< neV) among neutron scattering techniques allowing the direct measurement of the time-dependent intermediate scattering function  $S(q, t)$ , where  $q$  denotes the momentum transfer. NSE is well suited to investigate the dynamics of soft matter samples, such as polymers or proteins in solution.<sup>1</sup> Recently it has been

used to investigate protein dynamics and to understand its role in the functionality of the respective protein.<sup>2,3</sup> Typically, a comparatively high concentration of the respective biological sample in the order of 1 to 5 wt. % is necessary to achieve a good signal to noise ratio. These high concentrations increase the probability of a spontaneous aggregation (or agglomeration) of the sample, which is a clustering of dispersed particles sticking to each other. Usually, one wants to investigate the monomeric nanoparticles, and thus this aggregation

is a serious problem, since NSE measurement can take more than one day and a change in the sample aggregation state leads to unreliable NSE data. Moreover, aggregation depends on many parameters like sample purity and oxygen content of the solvent, which are difficult to control. Therefore, aggregation even differs from one sample mixture to another made under the same conditions. For this reason, *in situ* monitoring on a minute time scale of the sample is required to detect the aggregates formed.

Dynamic Light Scattering (DLS) is a well-suited method, since it has no influence on the neutron measurement and allows the user to get an informative overview of the sample aggregation state for subsequent time intervals in the minute time range. DLS or also known as photon correlation spectroscopy is commonly used in laboratories as a bench top method for analyzing dissolved nanoparticles or macromolecules. It enables to measure the diffusion coefficient of the dissolved particles caused by the Brownian motion. The obtained diffusion coefficient can be used to calculate the so called hydrodynamic radius, which is a measure for the size of a hard sphere, which has the same diffusion coefficient as the dissolved particle.<sup>4</sup> Since properly dissolved sample particles and the aggregates have different dimensions in size and also different diffusion coefficients, it is possible to distinguish between particles and aggregates. This approach also holds true for low concentrations of the aggregates due to the Rayleigh scattering law, which states that the intensity of the scattered light scales with the particle diameter to the sixth power. Therefore, for example, Li *et al.* used DLS to characterize protein aggregation.<sup>5</sup> Recently, Austin *et al.* used a commercial multi-angle dynamic light scattering setup equipped with three scattering angles to quantify various nanoparticle concentrations in a range from  $10^8$  to  $10^{14}$   $\text{ml}^{-1}$ .<sup>6</sup> In addition to size and concentration measurements, DLS can further be used for the study of internal dynamics and interactions, e.g., the dynamics of charged macromolecules<sup>7</sup> or interactions between proteins.<sup>8</sup>

Both scattering techniques, NSE and DLS, measure the intermediate scattering function directly and are complementary with respect to their  $q$ - and time-range. This feature makes both techniques attractive to use in combination for further analysis<sup>9–13</sup> and especially interesting for the study of protein dynamics.<sup>14–16</sup> In contrast to *ex situ* DLS measurements, the *in situ* DLS measurements will provide data to the very same sample and guarantees the same solvent and temperature conditions as in the NSE measurement. *In situ* DLS measurements have also been performed in combination with Small Angle Neutron Scattering experiments<sup>17–19</sup> and also recently an experimental setup offering one scattering angle was tested successfully at the J-NSE Phoenix spectrometer at the Heinz Maier-Leibniz Zentrum (MLZ).<sup>16,20</sup> Also the spin echo spectrometer IN15 at Institut Laue-Langevin supplies a sample changer allowing to perform *in situ* DLS with one scattering angle.<sup>13</sup>

Here, we report on a newly designed sample environment called *Bio-Oven* at the J-NSE Phoenix,<sup>21</sup> which involves an *in situ* DLS setup with three scattering angles. This multi-angle scattering setup guarantees a higher reliability and the option for a more extensive data analysis after the completed neutron measurement. Since it also provides two different laser wavelengths (red and green), the intermediate scattering function at six values of the momentum transfer  $q$ , ranging from 0.016 to 0.027  $\text{nm}^{-1}$  can be measured. A temperature control of the sample is provided by a temperature controlled air stream and two temperature sensors close to the sample

cuvettes. This provides an accurate temperature control, which is crucial for the temperature sensitive biological samples. The laser safety is guaranteed by a complete lightproof DLS setup and an additional laser safety interlock when opening it. The DLS setup is controlled via the neutron instrument control software NICOS, which is under continuous development at MLZ.

## II. MEASURING PRINCIPLES

DLS is a commonly used technique to characterize nanoparticles or macromolecules dissolved in a liquid and, in particular, also well suited to investigate polymers and proteins in solution.<sup>4,22,23</sup> Stetefeld *et al.* give a detailed introduction to this technique considering the fundamental theoretical aspects as well as the employed applications of DLS. This section includes only the basic principles of DLS and summarizes the work of Stetefeld *et al.*<sup>8</sup>

The scattering technique is based on the Brownian motion of the dissolved particles, a random movement caused by collisions of these particles with the fast moving molecules of the fluid due to thermal fluctuations. A basic setup includes a laser as a monochromatic, continuous and coherent light source, the fluid sample in a glass cuvette, a single photon detector, and a correlator card. Optomechanical elements are used to focus the laser beam on the sample and to collect the scattered light in a certain angle with respect to the incident laser beam. The momentum transfer  $q$  is given by formula (1) with the refractive index  $n$  of the solution, the vacuum wavelength  $\lambda_0$  of the laser, and the scattering angle  $\vartheta$ ,

$$q = \frac{4\pi n}{\lambda_0} \sin\left(\frac{\vartheta}{2}\right). \quad (1)$$

The scattered light waves interfere with each other and due to the random movement of the dissolved particles this can either result in constructive or destructive interference leading to a time-dependent intensity signal  $I(t)$  of the scattered light. This stochastic signal contains information about the particles movement over time and thus size. Basically, small particles move faster and as a consequence intensity fluctuations show up on a smaller timescale. In the homodyne detection method, where only scattered light reaches the detector, the stochastic intensity signal of the scattered light is analyzed with the normalized second order autocorrelation function  $g^{(2)}(q, \tau)$ , which correlates the intensity at times  $t$  and  $t + \tau$ ,

$$g^{(2)}(q, \tau) = \frac{\langle I(q, t)I(q, t + \tau) \rangle}{\langle I(q, t) \rangle^2}. \quad (2)$$

For the data analysis, the first order autocorrelation function  $g^{(1)}(q, \tau)$  can be calculated via the Siegert relation,

$$g^{(2)}(q, \tau) = 1 + \left| g^{(1)}(q, \tau) \right|^2. \quad (3)$$

The first order autocorrelation function is also known as the intermediate scattering function and can be modeled by a superposition of exponential decays with characteristic decay times  $\tau_i$ ,

$$g^{(1)}(q, \tau) = \sum_i^N A_i e^{-\tau/\tau_i}. \quad (4)$$

These characteristic decay times  $\tau_i$  extracted from stochastic fluctuations in light intensity can be directly related to the

momentum transfer  $q$  and the diffusion coefficient  $D$  as following:  $1/\tau_i = D_i q^2$ . Furthermore, the Stokes–Einstein Eq. (5) allows us to calculate the hydrodynamic radius  $r_{H,i}$  with known viscosity  $\eta$  and temperature  $T$  of the solvent for the corresponding diffusion coefficient  $D_i$ . It provides the radius of a hard sphere in solution, which diffuses as fast as the sample molecules,

$$r_{H,i} = \frac{k_B T}{6\pi\eta D_i} = \frac{16\pi n^2 k_B T \tau_i}{6\lambda_0^2 \eta} \sin^2\left(\frac{\vartheta}{2}\right). \quad (5)$$

For a monodisperse sample ( $N = 1$ ), a single exponential decay  $A_1 \cdot \exp(-\tau/\tau_1)$  can be used to fit the data and, thus, to estimate the size of the dissolved particles assuming only translational diffusion and a spherical shape.

Considering  $g^{(1)}(q, \tau)$  as a superposition of several decay times  $\tau_i$  the term  $A_i$  is the amplitude of the respective exponential decay. Therefore, for many  $N$ , the amplitudes  $A_i$  can be seen as a smooth continuous distribution  $G(\tau)$  of decay times  $\tau$ ,

$$g^{(1)}(q, \tau) = \int G(\tau') e^{-\tau/\tau'} d\tau'. \quad (6)$$

A size distribution of hydrodynamic radii can be obtained directly from  $G(\tau)$  by using the Stokes–Einstein equation. However, to obtain  $G(\tau)$  from formula (6), one has to calculate the inverse Laplace transformation of  $g^{(1)}(q, \tau)$ , which is an ill-posed problem. The CONTIN algorithm by Provencher can be used to calculate the distribution  $G(\tau)$  under the assumption of a smooth distribution. This is implemented in an algorithm used for data treatment as a weighted least square problem with an additional quadratic term for smoothness.<sup>24</sup>

### III. EXPERIMENTAL SET-UP

#### A. Design

The new sample environment reported here consists of two parts: A light-proof aluminum cylindrical casing and an inset, which is fixed to the removable top cover of the casing and carrying the optical components needed for the DLS measurements. The temperature is controlled through an air stream entering the casing on its bottom side and exiting it at the top. Two temperature sensors are placed in drillings next to the two sample cuvettes for monitoring.

Figure 1(a) shows the schematic cross section of the removable inset and Fig. 1(b) a photograph of the inset on an external holder. This inset includes two fixtures, one for the main sample cuvette and one for a second sample cuvette (for instance, a reference sample or a buffer solution). Figure 1(c) shows a photograph of the Bio-Oven mounted at the sample stage of the J-NSE instrument and in Fig. 1(d) a schematic top view is presented. The Bio-Oven is placed between the superconducting magnetic coils, directly behind the  $\pi$ -flipper. The yellow arrows in Figs. 1(a) and 1(d) indicate the neutron beam path. The inset is located inside the lightproof cylindrical casing, which has a reduced aluminum thickness of 1 mm at the height where the neutron beam passes in order to increase the neutron transmission through the aluminum casing. Both cuvettes can be moved into the neutron beam using the motorized translation stage of the J-NSE instrument by moving the whole sample holder in height.

For the optical alignment of the free space DLS setup or sample changing, the inset is taken out of the cylindrical casing as shown in Fig. 1(c) and put onto an external holder as shown in Fig. 1(b). The restricted available place for the DLS setup and laser

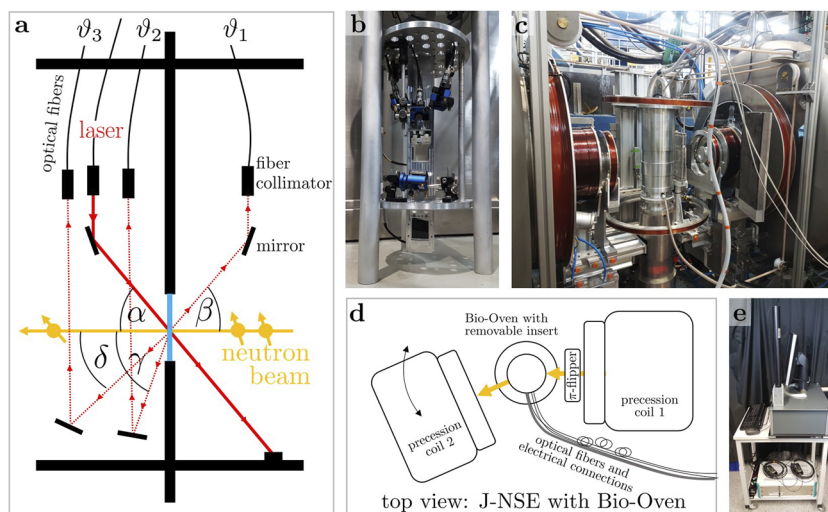


**FIG. 1.** (a) Schematic cross section of the newly developed sample environment, which allows *in situ* DLS measurements with three scattering angles at the J-NSE Phoenix at MLZ. The laser beam (red solid line) leaves the lens of the fiber collimator (black rectangle) and is guided by a mirror to the sample. The scattered light (red dashed lines) is redirected by mirrors and collected by collimators on the top. The neutron flight path is indicated with yellow arrows. (b) Photograph of the inset put onto an external holder. (c) Photograph of the J-NSE instrument with the mounted Bio-Oven, which is a light proof casing containing the inset shown in (a) and (b). (d) Schematic top view of the J-NSE instrument. (e) Photograph of the mobile cart carrying all components used for DLS measurements including an optical bench with laser and optics, detectors, correlator cards, laser safety interlock, and a PC.

safety was the main challenges in the design of this setup. Moreover, the usage of non-magnetic materials was essential, since neutron spin echo spectroscopy uses the polarization of the neutron spin. Magnetic materials in the vicinity of the beam path cause a depolarization of the neutron beam. Therefore, the structural elements are made out of ALMg3 and all opto-mechanical elements used are nonmagnetic.

The inset includes two circular supporting plates, which carry the optical elements necessary for the *in situ* DLS. Light scattering is possible for the upper cuvette, and the light scattering plane is arranged in a way that it is orthogonal to the neutron scattering plane. As schematically drawn in Fig. 1(a), three scattering angles are installed. The laser light is guided by a polarization maintaining single mode fiber to the Bio-Oven and focused with a lens of a fiber collimator and a mirror onto the sample. The scattered light is coupled with mirrors and collimator lenses into optical fibers, which guide the light to single photon detectors. The scattering angles, which could be achieved, were mostly restricted by the available space and the size of the available non-magnetic optical components. Mirror mounts were purchased from LIOP-TEC GmbH, Radevormwald, Germany (custom-made out of non-magnetic materials based on the model SR050). Single-mode fibers and fiber collimator lenses were bought from Schäfer + Kirchoff GmbH, Hamburg, Germany (Table S1 in the supplementary material).

The three scattering angles  $\vartheta_1$ ,  $\vartheta_2$ , and  $\vartheta_3$  depend on the angles  $\alpha$ ,  $\beta$ ,  $\gamma$ , and  $\delta$  drawn in Fig. 1(a) and the refractive index of the sample solution  $n_s$ . They can be determined by formulas (7)–(9) (for derivation see Fig. S1 in the supplementary material),

$$\vartheta_1 = \sin^{-1}\left(\frac{n_{\text{air}}}{n_s} \sin \alpha\right) + \sin^{-1}\left(\frac{n_{\text{air}}}{n_s} \sin \beta\right), \quad (7)$$

$$\vartheta_2 = 180^\circ - \sin^{-1}\left(\frac{n_{\text{air}}}{n_s} \sin \alpha\right) - \sin^{-1}\left(\frac{n_{\text{air}}}{n_s} \sin \gamma\right), \quad (8)$$

$$\vartheta_3 = 180^\circ - \sin^{-1}\left(\frac{n_{\text{air}}}{n_s} \sin \alpha\right) - \sin^{-1}\left(\frac{n_{\text{air}}}{n_s} \sin \delta\right). \quad (9)$$

The measured values are  $\alpha = 55^\circ$ ,  $\beta = 55^\circ$ ,  $\gamma = 65^\circ$ ,  $\delta = 40^\circ$  and so the scattering angles can be calculated with  $n_{\text{air}} = 1.00$  and  $n_s = 1.33$  assuming water as a typical sample solvent. Using these values the scattering angles are  $\vartheta_1 \approx 75^\circ$ ,  $\vartheta_2 \approx 100^\circ$ , and  $\vartheta_3 \approx 115^\circ$ . A different approach to determine the scattering angles is a DLS measurement using reference particles with a known size. The resulting momentum transfer values from Eq. (1) are shown in Table I for a green and red emitting laser, which are used for this setup. The uncertainty of the calculated  $q$ -values obtained by Gaussian error propagation is  $\sim 6\%$ , assuming a maximum error of  $5^\circ$  in both mea-

**TABLE I.** Achievable momentum transfers  $q$  in units of  $\text{nm}^{-1}$  resulting from the three installed scattering angles and two different laser wavelengths.

	$\vartheta_1 = 75^\circ$	$\vartheta_2 = 100^\circ$	$\vartheta_3 = 115^\circ$
$\lambda_{\text{red}} = 632.8 \text{ nm}$	0.016	0.020	0.022
$\lambda_{\text{green}} = 532.1 \text{ nm}$	0.019	0.024	0.027

sured angles and a negligible error in the refractive index and laser wavelength.

## B. The modular setup of the Bio-Oven

The other components needed to perform DLS measurements are located on a wheeled cart next to the instrument, which is shown in Fig. 1(e).

A lightproof casing includes two different lasers and other optical elements for polarization control, intensity adjustment, laser safety and fiber incoupling (shown in Fig. S2 in the supplementary material). Either a He–Ne laser with a wavelength of 632.8 nm and a power of 22 mW (Model 1145/P by JDS Uniphase, Eningen, Germany) or a diode-pumped laser with a wavelength of 532.1 nm and a power of 100 mW (Cobolt Samba 150 532 nm by HÜBNER Photonics GmbH, Kassel, Germany) can be coupled into the fiber. A mirror placed on a motorized translational stage allows switching between both. A filter wheel is used to adjust the intensity of the incident laser light. It is equipped with eleven neutral density filters with a transmission ranging from 0.1% to 75% and an additional open position (100% transmission). Furthermore, the casing includes two beam blockers and a shutter for laser safety reasons.

The single photon detectors SPCM CD 3296 by Excelitas Technologies GmbH and Co. KG, Wiesbaden, Germany are located in an extra casing. One fiber is connected directly with one of the detectors, whereas a filter wheel is installed between the other two fibers and detectors in order to reduce the intensity if necessary. A full list of the collimators and optical fibers used can be found in Table S1 in the supplementary material.

An electric cabinet hosts the correlator cards, a personal computer and the electric management for the laser safety interlock. The photon hardware correlator is based on a field-programmable gate array development board (FPGA SP605 board by Xilinx Inc., San Jose, United States). The implementation from Kalinin *et al.* was used.<sup>25</sup> The measurement software is based on python and developed in the framework of the Neutron Instrument Control Software NICOS. This way, it can be controlled by an external computer and integrated into the neutron measurement.

The laser safety is independent of the software and guaranteed through contact switches on top of the Bio-Oven. This mechanism takes care that no laser light leaves the laser box when the Bio-Oven is not fully closed. A more detailed and schematic overview of the whole setup is shown in Fig. S3 in the supplementary material.

The temperature of the cuvettes is controlled with an air stream generated by the commercial instrument ThermoJet ES Precision Temperature Cycling System by SP Scientific, Warminster, PA, United States. Its air stream temperature can be set from  $-80^\circ$  to  $225^\circ$  and the airflow can be set from 2.3 to 9.4 L/s. However, the operational temperature of the Bio-Oven lies between 5 and  $70^\circ\text{C}$ , limited due to the condensation of water at low temperatures and increasing thermal fluctuations at higher temperatures. The air is guided from the apparatus to the Bio-Oven with a hose connected to the airshaft at the bottom of the Bio-Oven and leaves through the output on the top cover. For a better thermal insulation, a plate out of MONOLUX<sup>®</sup>-800 is mounted between the Bio-Oven and the J-NSE sample stage. For the temperature read-out the Cryogenic Temperature Controller 336 by Lake Shore Cryotronics,

Inc., Westerville OH, United States is used. A long-term test over hours showed a constant temperature with a standard deviation of  $\sim 0.15^\circ\text{C}$  (see Fig. S4 in the [supplementary material](#)).

#### IV. RESULTS

##### A. Dynamic light scattering measurements with silica nanospheres

The Dynamic Light Scattering setup was aligned and characterized using silica nanospheres ( $\text{SiO}_2$ ). The samples were bought from nanoComposix, San Diego CA, United States in three different particle sizes with diameters of 20, 100, and 300 nm. The particles were dissolved in deionized water to obtain a concentration of 1.0 mg/ml for all three samples. The particle radii measured by transmission electron microscopy (TEM) can be found in [Table II](#). The samples were filled in quartz glass cuvettes from Hellma GmbH and Co. KG, Müllheim, Germany with a sample thickness of 4.0 mm. The DLS setup was aligned by means of the particles with 100 nm size and was not optimized or realigned for other samples after sample changing. The alignment process maximized the absolute intensities under the boundary condition of a meaningful autocorrelation function.

A measurement duration of 120 s was used for each sample. All autocorrelation functions  $g^{(2)}(q, \tau)$  were recorded at the same time and show an intercept at the y-axis above 0.9 and exhibit the shape of a single exponential decay as expected. Using the Siegert relation (3) the first order autocorrelation functions  $g^{(1)}(q, \tau)$  of both laser colors were fitted with a single exponential decay of the form  $y(\tau) = A_1 \times \exp(-\tau/\tau_1)$ . [Figure 2](#) shows the recorded autocorrelation functions of the 100 nm sample with their fit functions. The nanoparticles of 20 and 300 nm diameter yield similar curves (see Fig. S5).

Using the Stokes–Einstein Eq. (5) the hydrodynamic radii  $r_H$  were calculated. The temperature was constant at  $T = 20^\circ\text{C}$  where the viscosity of water amounts to  $\eta = 1.00 \text{ mPa s}$ .<sup>26</sup> The refractive index of water is assumed to be  $n = 1.33$  for the green ( $\lambda = 532.1 \text{ nm}$ ) and the red laser ( $\lambda = 632.8 \text{ nm}$ ).<sup>27</sup>

In order to compare and discuss the results the same samples were measured with a commercial instrument, the Zetasizer Nano S by Malvern Panalytical GmbH, Kassel, Germany, also in a quartz glass cuvette by Hellma with a lightpath of 10.0 mm at a temperature of  $20^\circ\text{C}$ . The fixed scattering angle of the Zetasizer device amounts to  $\vartheta_{\text{Zetasizer}} = 173^\circ$  and it used also a He–Ne laser with a wavelength of 632.8 nm. Neglecting the refraction yields a momentum

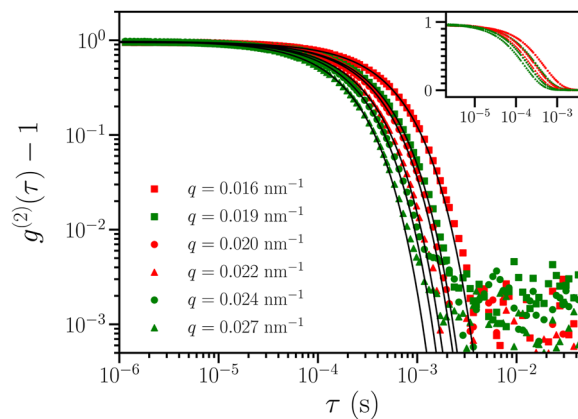


**FIG. 2.** Second order autocorrelation functions of 100 nm silica nanospheres dissolved in water using all three scattering angles simultaneously and two laser sources successively ( $\lambda_0 = 532, 633 \text{ nm}$ ) resulting in six different momentum transfer values  $q$ . The green and red plotted symbols indicate the measurements with the respective laser color used and the shape of the symbol the scattering angle (rectangle:  $\vartheta_1 = 75^\circ$ , circle:  $\vartheta_2 = 100^\circ$ , triangle:  $\vartheta_3 = 115^\circ$ ). Single exponential decay functions were fitted using the Siegert relation (black solid lines). Inset: Plot with the linear y-axis.

transfer of  $q_{\text{Zetasizer}} = 0.026 \text{ nm}^{-1}$ . The fit procedure and calculation of  $r_H$  were done manually with the raw  $g^{(2)}(q, \tau)$  data of the Zetasizer in the same way as with the data from the Bio-Oven setup. All determined hydrodynamic radii are listed in [Table II](#) together with the radii obtained by TEM.

##### B. Static light scattering with silica nanospheres

The possibility to perform static light scattering was explored, since setup provides six different  $q$ -values by using two different laser wavelengths and the scattering angles. In this case, the time dependence of the signal is no longer of interest, but the absolute intensity  $I(q)$  of the scattered light in dependence of the momentum transfer  $q$  contains structural information e.g., form and size, of the dissolved particles. For normalization of the measured intensities at different angles, a sample with scatterers of a small size was used, whose scattered intensities are expected to be independent of the momentum transfer and, therefore, can be used for the normalization. Here, the protein Bovine serum albumin (BSA)

**TABLE II.** Determined hydrodynamic radii of silica nanospheres in different sizes measured with the Bio-Oven and the commercial instrument Zetasizer for comparison. The radii of the particles measured with transmission electron microscopy (TEM) as given by the manufacturer are shown in the last column.

	$r_H$ (nm)						Zetasizer	$r$ (nm)
	Bio-Oven $\vartheta_1 = 75^\circ$		Bio-Oven $\vartheta_2 = 100^\circ$		Bio-Oven $\vartheta_3 = 115^\circ$			
	$\lambda = 532 \text{ nm}$	$\lambda = 633 \text{ nm}$	$\lambda = 532 \text{ nm}$	$\lambda = 633 \text{ nm}$	$\lambda = 532 \text{ nm}$	$\lambda = 633 \text{ nm}$		
20 nm 1.0 mg/mL	$11.1 \pm 1.5$	$11.8 \pm 1.6$	$11.8 \pm 1.5$	$14.9 \pm 1.9$	$11.3 \pm 1.3$	$14.7 \pm 1.8$	$13.0 \pm 1.6$	$11.1 \pm 1.6$
100 nm 1.0 mg/mL	$53 \pm 7$	$55 \pm 7$	$51 \pm 6$	$53 \pm 7$	$50 \pm 6$	$51 \pm 6$	$54 \pm 7$	$49 \pm 6$
300 nm 1.0 mg/mL	$141 \pm 19$	$138 \pm 18$	$152 \pm 19$	$142 \pm 17$	$157 \pm 19$	$140 \pm 16$	$141 \pm 17$	$139 \pm 6$

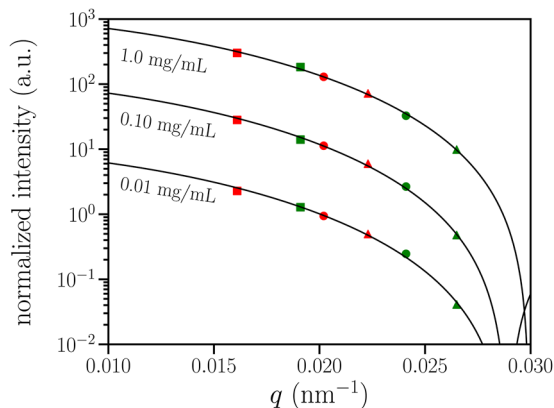


**FIG. 3.** Normalized scattered intensities of 300 nm silica nanospheres dissolved in water for three different concentrations in dependence of the momentum transfer  $q$ . The green and red symbols correspond to the respective laser color, which was used to measure the data. The shape of the symbol indicates the respective scattering angle: rectangle:  $\vartheta_1 = 75^\circ$ , circle:  $\vartheta_2 = 100^\circ$ , triangle:  $\vartheta_3 = 115^\circ$ . Black solid lines are fit functions using the form factor  $F(q, R)$  of a hard sphere and provide radii between 150 and 155 nm.

dissolved in water was used with a concentration of 60 mg/ml for the normalization.

Silica nanospheres with a diameter of 300 nm were measured in water with three different concentrations ranging from 0.01 to 1.0 mg/ml. The measured count rates  $CR_{300\text{ nm}}$  reach over several orders of magnitude depending on concentration and momentum transfer. Therefore, the laser intensity was reduced with different neutral density filters to avoid a saturation of the detector. The measured signal  $CR_{300\text{ nm}}$  was normalized with the signal of BSA  $CR_{\text{BSA}}$ , respectively, for each momentum transfer  $q$  and corrected by the transmission  $T$  of the neutral density filter used to reduce the laser intensity,

$$I_{\text{norm}} = \frac{CR_{300\text{ nm}}}{CR_{\text{BSA}} \cdot T}. \quad (10)$$

The resulting normalized intensities are plotted in Fig. 3 vs the momentum transfer  $q$  using the values from Table I. The data were fitted with the function  $I(q) = A \cdot F(q, R)^2$  using the form factor of a hard sphere with radius  $R$ , which is given by Eq. (11),

$$F(q, R) = \frac{3(\sin(qR) - qR \cos(qR))}{(qR)^3}. \quad (11)$$

The obtained parameters from the fit functions are shown in Table III.

**TABLE III.** Fit parameters of the static light scattering experiment with 300 nm silica nanospheres shown in Fig. 3.

	0.01 mg/mL	0.10 mg/mL	1.0 mg/mL
A	$10.1 \pm 0.7$	$120 \pm 6$	$1142 \pm 55$
R in nm	$154.8 \pm 0.9$	$155.3 \pm 0.6$	$150.0 \pm 0.7$

### C. Long-term test with a protein sample

A DLS measurement series over a typical duration of a spin echo beam time on a realistic sample was carried out. This test was performed at the NSE instrument, but without the neutron beam being present during a reactor break period. The investigated sample was a solution of horse-heart apomyoglobin in heavy water. The apomyoglobin solution was prepared by dissolving the protein pellets in heavy water (99.9 at. % D) and filtered using 100 nm syringe filters (Anotop Filter–Whatman) to remove aggregates. Deuterium chloride was added to change the folding state of the protein ( $pD = 4$ ). The final concentration was 30 mg/ml, and the sample was filled into a 4.0 mm path length quartz glass cuvette. Measurements were carried out over a duration of five days at a fixed temperature of  $10^\circ\text{C}$ . A single DLS measurement amounted to 300 s and the green and red laser were used alternately.

A typical measurement of both lasers is shown in the upper part of Fig. 4, which was recorded one day after the start. The scattered intensity signal is in the low kHz regime or even below, since protein is very small in size ( $\approx 1\text{ nm}$ ). The signal-to-noise ratio and also natural misalignment due to thermal changes and vibrations in the floor lead to low intercepts in the range of 0.4 to 0.8 in the autocorrelation functions  $g^{(1)}(q, \tau)$ .

The angle  $\vartheta_3 = 115^\circ$  in combination with the red laser resulted in an unusual autocorrelation functions with a reproducible oscillatory feature at the second decay (see top most curve in Fig. 4).

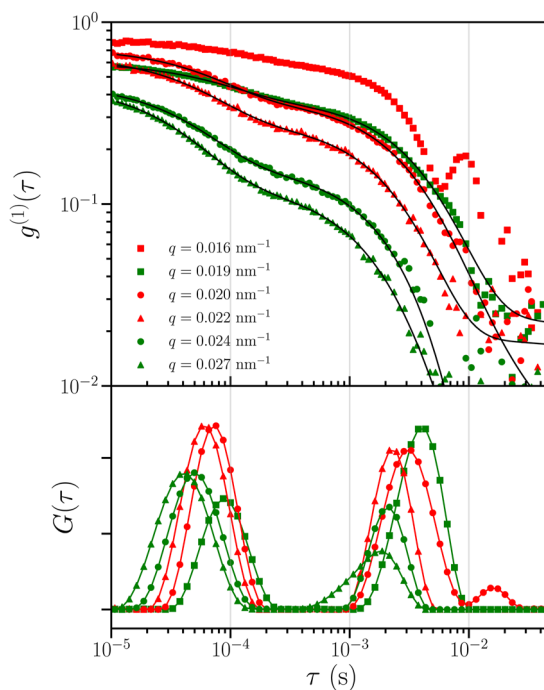


**FIG. 4.** Top: First order autocorrelation function of the 30 mg/ml apomyoglobin solution in the Bio-Oven recorded one day after the measurement beginning. The black solid lines are fit functions using the CONTIN algorithm by Provencher. Bottom: Obtained distribution  $G(\tau)$  from the CONTIN fit of  $g^{(1)}(q, \tau) = \int G(\tau') \exp(-\tau/\tau') d\tau'$ .

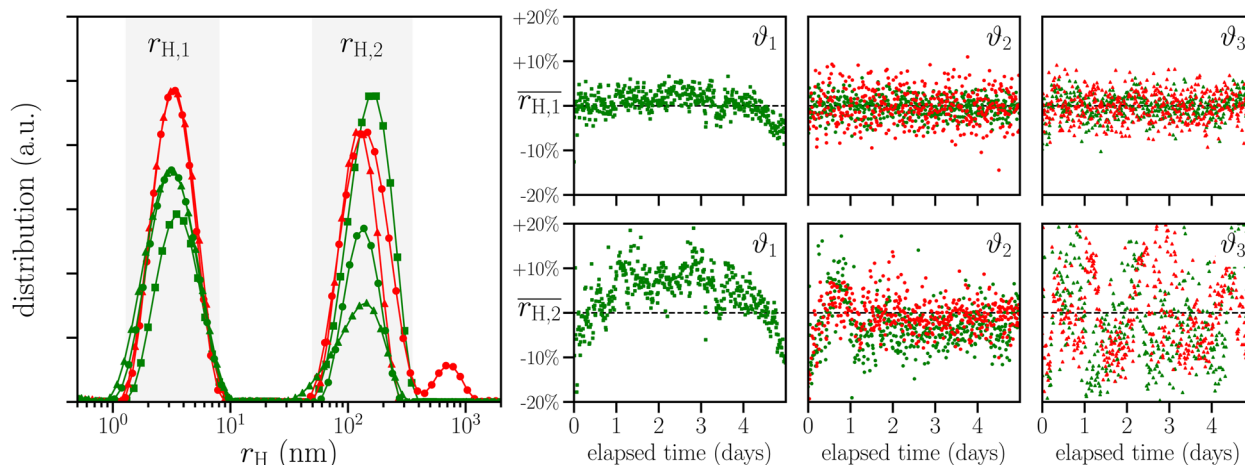


**FIG. 5.** Left: Distribution of the hydrodynamic radii obtained from the same measurement shown in Fig. 4 by using the Stokes-Einstein Eq. (5). No volume or mass correction was applied. Right: Temporal variation of  $r_{H,1}$  and  $r_{H,2}$  obtained from the three scattering angles during the whole measurement time over five days. For  $\vartheta_1$  in combination with the red laser no meaningful radii could be extracted due to the oscillation feature in  $g^{(1)}(q, \tau)$  as shown in Fig. 4.

Kang and Sadakane previously reported on oscillations in autocorrelation functions caused by an external electric field for lysozyme solutions.<sup>28</sup> However, this feature was not observed at the very same scattering angle under usage of the green laser and thus the origin is not clear up until now.

The CONTIN algorithm by Provencher was used to fit the other five meaningful autocorrelation functions and produced a distribution of decay times  $G(\tau)$ , which is shown exemplary for one measurement in the lower part of Fig. 4. Furthermore, these decay times can be converted into respective hydrodynamic radii using Eq. (5) with known scattering geometry, viscosity and temperature of the sample. The viscosity of the sample was determined to  $\eta = 2.1$  mPa s using the rolling ball viscometer Lovis 2000 M/ME from Anton Paar ( $T = 10^\circ\text{C}$ ). On the left hand side of Fig. 5 the resulting hydrodynamic radii distribution is shown, which is obtained by converting the  $G(\tau) \text{ vs } \tau$  datasets to  $G(\tau) \text{ vs } r_H$  datasets using Eq. (5). The graph does not represent an actual volume or mass distribution, since size dependency of the scattered light intensity was not taken into account, which needs to be considered to quantify volume fractions of different species. The  $r_{H,1}$  value is in the order of 3 nm and is a reasonable value for the monomeric unfolded protein. A second species with a  $r_{H,2}$  value in the order of 100 nm could represent aggregates of the protein.

These distributions suggest that the data can be described by a double exponential decay. For this reason, the data over the whole measurement time of five days was evaluated by fitting the first order autocorrelation function with a double exponential decay of the form  $y(\tau) = A_1 \cdot \exp(-\tau/\tau_1) + A_2 \cdot \exp(-\tau/\tau_2)$ . Using both decay times from the fit function two hydrodynamic radii were calculated as described above. The time dependent variation of these hydrodynamic radii  $r_{H,1}$  and  $r_{H,2}$  were plotted vs the elapsed time since measurement start on the right hand side of Fig. 4. The time dependent behavior of  $r_{H,2}$  for different scattering angles is noteworthy in contrast with a rather temporally constant  $r_{H,1}$ . The maximum

deviation from the mean  $\overline{r_{H,2}}$  amounts to 20%. No increasing trend was observed among the hydrodynamic radii, so the sample can be regarded as stable over time.

#### D. First neutron measurement with *in situ* DLS measurements

At first measurements with a graphite powder reference sample were performed using the DLS position of the new sample environment and compared with the reference sample position. The reference sample was in a quartz glass cuvette with a sample thickness of 4 mm. The chosen momentum transfer for the reference sample was  $q = 0.1 \text{ \AA}^{-1}$  and Fourier times ranging from 0.50 up to 50 ns were measured. No significant differences between the DLS position in the Bio-Oven and the reference position could be observed as shown in Fig. S6 in the [supplementary material](#).

Afterward, the Bio-Oven was used for a first neutron measurement with DLS on the protein sample apomyoglobin (24 mg/ml) in 3M guanidinium chloride. It was also filled in the 4.0 mm quartz glass cuvette. The data of the neutron measurement seemed trustworthy and the new Bio-Oven showed no indications to have impact on the neutron experiment.

The DLS measurement duration was set to 300 s and only the red laser was used. Only two scattering angles ( $\vartheta_1 = 75^\circ$  and  $\vartheta_3 = 115^\circ$ ) were installed at that time. Figure 6 shows some of the recorded autocorrelation functions  $g^{(2)}(q, \tau)$ .

For both scattering angles, two characteristic decay times could be observed in all autocorrelation functions and, thus, were fit with a superposition of exponential decays providing  $\tau_1$ ,  $\tau_2$ ,  $A_1$ , and  $A_2$ . It turns out that the fit parameters of the first decay stay nearly constant over the whole measurement duration, but the second decay shows some nonsystematic fluctuations. A closer look at the extracted  $\tau_2$  at  $q = 0.022 \text{ nm}^{-1}$  over time shows a slight continuous linear increase. The amplitude ratio  $A_2/(A_1 + A_2)$  is also of interest, because it is

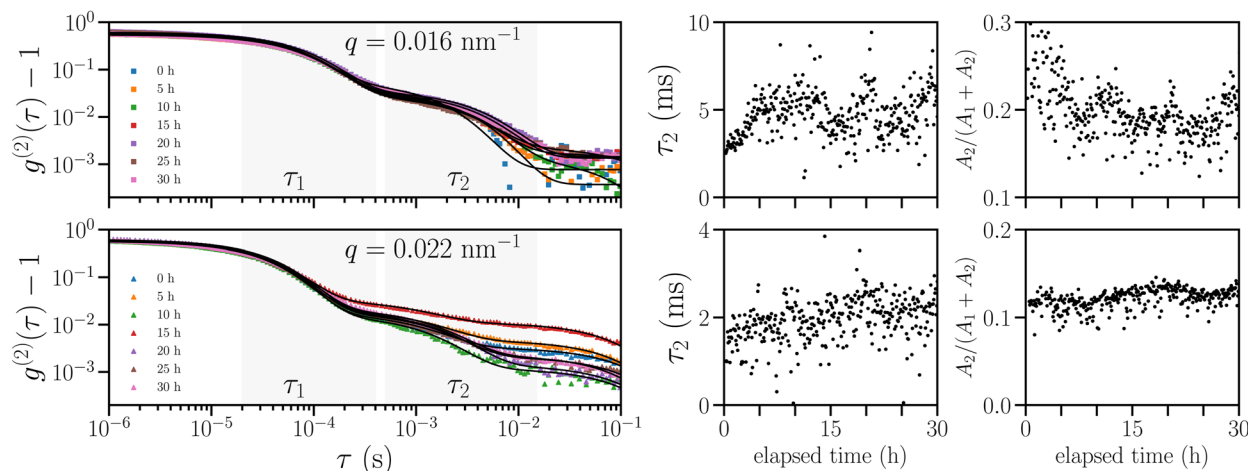


**FIG. 6.** Recorded second order autocorrelation functions  $g^{(2)}(q, \tau)$  of the protein sample apomyoglobin during the first neutron measurement with two scattering angles  $\vartheta_1 = 75^\circ$  (upper graphs) and  $\vartheta_3 = 115^\circ$  (lower graphs). Here, as an example 0, 5, 10, . . . , 30 h after the neutron measurement start. The data were fit with a superposition of the exponential decays. The extracted  $\tau_2$  and normalized amplitudes of the second decay are plotted vs time to detect a possible change in the aggregation state of the sample.

proportional to the volume fraction of particles with larger size. Also here a slight increase is observed over time, but only in the second scattering angle with  $q = 0.022 \text{ nm}^{-1}$ .

## V. DISCUSSION AND OUTLOOK

The newly developed sample environment Bio-Oven for the Jülich Spin Echo Spectrometer J-NSE Phoenix features a fine temperature control and a three angle two laser colors *in situ* dynamic light scattering setup. It is in routine user operation now and has proven its reliability. It follows a similar fiber based modular concept as shown in Balacescu *et al.*<sup>20</sup> It takes into account that spin echo measurement times on one sample are often on the order of hours to days, so a multi-position sample changer is less important than in small angle neutron scattering (SANS) beam times. Instead, a fine temperature control is required, which is provided by the presented Bio-Oven. Its *in situ* DLS option is constructed in a way that always two scattering angles are aligned independent of the thickness of the cuvette. These are the scattering angles on the left side in reflection geometry to the incoming laser beam [see Fig. 1(a)]. The third scattering angle needs some adjustment depending on the thickness of the cuvette in use. This provides the possibility to switch between cuvettes of different thicknesses without the need for re-alignment for at least two scattering angles. A similar concept has been followed by Schmid *et al.* for an *in situ* DLS at a future SANS instrument.<sup>18</sup> Here, a big optical table is used as a base on which the pre-aligned DLS setup is fixed together with a 96 position sample changer. This also minimizes optical alignment needs when switching to the *in situ* DLS option. Just the optical table as a whole has to be aligned to the neutron beam. This is also true for the Bio-Oven presented here. The sample stage of the J-NSE Phoenix moves vertically to change the sample.

The *in situ* DLS setup has been characterized first with silica nanospheres. Here, dynamic light scattering and even static light scattering could be performed. The results could be compared with values obtained by standard bench top lab instruments such as the Malvern Zetasizer. The obtained hydrodynamic radii in Table II are consistent with one another and, in general, show good agreement with the measured values obtained by the commercial device. The radius of gyration as determined from transmission electron microscopy images is given for a reference in Table II and furthermore confirms our measurements.

The static light scattering experiment with the silica nanospheres with a nominal diameter of 300 nm showed that it is basically possible to perform meaningful static light scattering with six different momentum transfer values  $q$ . The fit functions describe the recorded data well and also the obtained fit parameters of Table III are in good agreement with the nominal values supplied by the manufacturer of the nanoparticles. The amplitude  $A$  increases linearly with the concentration and the radius  $R$  reflects the size of the nanoparticles remarkably well.

However, these measurements were made with rather large particles and real samples are typically one or two orders of magnitude smaller. This is why a realistic protein test sample has been employed to perform a long term test of the Bio-Oven setup.

The collected autocorrelation curves of the protein sample apomyoglobin could be fitted either with a CONTIN algorithm or with a double exponential decay function. The first approach provides a realistic size distribution plot at all times during the neutron measurements and the second approach leads to a data reduction, which makes it simpler to set limits for events such that an e-mail is sent out to the actual user of the current beam time in order to raise awareness that the sample aggregation state has changed above these limits. The implementation of the Bio-Oven in the instrument

control software allows here for many options that the user can choose from.

Figure 4 shows a typical set of autocorrelation functions recorded one day after the measurement beginning. The observed differences between the measurements with the red and green laser can possibly be explained due to different scattering volumes. A different beam displacement is caused at the air-glass-solvent interface using two lasers, because the refractive index  $n(\lambda)$  depends on the wavelength. The difference was theoretically calculated to approximate  $8\ \mu\text{m}$ , which is significantly below the beam diameter and, therefore, the scattering volume only changes slightly.

Due to high concentrations of the apomyoglobin sample of  $30\ \text{mg/ml}$  also the phenomenon of multiple scattering can finally not be excluded to impact the measurements. Furthermore, for a quantitative analysis of the DLS correlation functions the phenomena related to collective effects have to be kept in mind at higher sample concentrations. In the proximity of peaks in the structure factor  $S(q)$ , relaxation times get large [i.e.,  $1/\tau \propto 1/S(q)$ ], known as “de Gennes narrowing.”<sup>29</sup> At high concentrations and very low  $q$  in DLS compared with NSE, it is furthermore possible that collective dynamics are probed at the DLS length scale at higher concentration, while single particle dynamics on the much smaller local length scales of NSE is relevant, which has to be taken into account for quantitative modeling of the data. Nevertheless, the long-term test suggests that the sample stayed stable over the whole duration of five days, since obtained hydrodynamic radii of one specific  $q$ -value stays constant with respect to the usual long term fluctuations and with respect to the uncertainty of measurement.

The recorded autocorrelation functions from the first *in situ* DLS measurements in combination with neutron scattering were made with an earlier version of the setup that only included two scattering angles. The Bio-Oven was comparable to a standard sample holder in terms of NSE performance and showed no change in the resolution function of the spin echo instrument J-NSE. This confirmed that the Bio-Oven has no influence on the spin echo data. In fact, the aggregation state of the sample could be monitored over hours and a slow aggregation process could be detected, which did not prove relevant for the spin echo data quality due to its small volume percentage.

It is up to the experiment leader to choose whether one wants to use only one laser color or one scattering angle or whether to employ only limits on the transmission of the sample. One can also program the frequency and the duration of the individual dynamic light scattering measurements. The recorded data can be processed online or can be downloaded remotely from any client connecting to the instrument control software NICOS of the spin echo instrument J-NSE.

In conclusion, we demonstrate the features of the newly developed sample environment Bio-Oven for the J-NSE Phoenix spin echo spectrometer at the MLZ. It provides temperature control for two sample cuvettes between  $5$  and  $70\ ^\circ\text{C}$ . It allows us to measure DLS curves at three scattering angles simultaneously with two laser colors subsequently *in situ* and will now serve as a routine sample environment for biological samples, which require fine temperature control. We show that the aggregation state of a realistic protein sample can be monitored over hours while having no negative influence on the spin echo measurements. In the future, one could use this fiber-based platform for implementing

other optical-based measurement techniques *in situ* e.g., Ultraviolet-Visible spectroscopy.

## SUPPLEMENTARY MATERIAL

The supplementary material includes Fig. S1 showing the calculation of the scattering angles using geometric relations, the complete list of the optical components used (see Table S1), and a view into the laser housing (Fig. S2). Furthermore, it provides a schematic drawing of the entire *in situ* setup in Fig. S3. Figure S4 shows the temperature stability at the sample cell over a 15 h period. Figure S5 reports the DLS data recorded for the silica spheres with 20 and 300 nm nominal diameter. Finally, Fig. S6 shows the reference spin echo measurement with a graphite powder sample in the sample cell of the Bio-oven.

## ACKNOWLEDGMENTS

We gratefully acknowledge the construction work of Nils Lumma. In part, this work was financially supported through the BMBF Project No. 05K16PA1.

## AUTHOR DECLARATIONS

### Conflict of Interest

The authors have no conflicts to disclose.

## Author Contributions

**F. Vögl:** Conceptualization (equal); Data curation (lead); Formal analysis (equal); Investigation (equal); Methodology (equal); Resources (equal); Software (equal); Validation (equal); Visualization (lead); Writing – original draft (lead); Writing – review & editing (lead). **L. Balacescu:** Data curation (lead); Formal analysis (equal); Investigation (lead); Methodology (lead); Project administration (equal); Validation (equal); Visualization (lead); Writing – original draft (lead); Writing – review & editing (equal). **O. Holderer:** Data curation (equal); Investigation (equal); Project administration (equal); Visualization (equal); Writing – review & editing (equal). **S. Pasini:** Data curation (equal); Resources (equal); Writing – review & editing (equal). **S. Staringer:** Methodology (equal); Resources (lead); Writing – review & editing (supporting). **G. Brandl:** Data curation (equal); Software (lead); Writing – review & editing (equal). **V. Ossovy:** Resources (lead); Software (equal); Writing – review & editing (supporting). **H. Feilbach:** Conceptualization (equal); Resources (equal); Writing – review & editing (equal). **P. Müller-Buschbaum:** Conceptualization (equal); Funding acquisition (equal); Project administration (equal); Validation (equal); Writing – review & editing (equal). **A. M. Stadler:** Conceptualization (equal); Funding acquisition (equal); Project administration (equal); Supervision (equal); Validation (lead); Visualization (equal); Writing – review & editing (equal). **J. Fitter:** Conceptualization (equal); Project administration (lead); Validation (lead); Writing – review & editing (equal). **T. E. Schrader:** Conceptualization (lead); Funding acquisition (lead); Project administration (lead); Supervision (lead); Validation (lead); Visualization (equal); Writing – original draft (equal); Writing – review & editing (lead).

## DATA AVAILABILITY

Data underlying the results presented in this paper are not publicly available at this time but may be obtained from the authors upon reasonable request.

## REFERENCES

- <sup>1</sup>D. Richter, M. Monkenbusch, A. Arbe, and J. Colmenero, *Neutron Spin Echo in Polymer Systems* (Springer, 2005) pp. 1–221.
- <sup>2</sup>R. Biehl, M. Monkenbusch, and D. Richter, *Soft Matter* **7**, 1299 (2011).
- <sup>3</sup>L. Haris, R. Biehl, M. Dulle, A. Radulescu, O. Holderer, I. Hoffmann, and A. M. Stadler, *Int. J. Mol. Sci.* **23**, 6969 (2022).
- <sup>4</sup>B. J. Berne and R. Pecora, *Dynamic Light Scattering: With Applications to Chemistry, Biology, and Physics* (Dover Publications, Inc., 2000).
- <sup>5</sup>Y. Li, V. Lubchenko, and P. G. Vekilov, *Rev. Sci. Instrum.* **82**, 053106 (2011).
- <sup>6</sup>J. Austin, C. Minelli, D. Hamilton, M. Wywijas, and H. J. Jones, *J. Nanopart. Res.* **22**, 108 (2020).
- <sup>7</sup>M. Muthukumar, *Proc. Natl. Acad. Sci. U. S. A.* **113**, 12627 (2016).
- <sup>8</sup>J. Stetefeld, S. A. McKenna, and T. R. Patel, *Biophys. Rev.* **8**, 409 (2016).
- <sup>9</sup>F. Horkay, P. Falus, A.-M. Hecht, and E. Geissler, *J. Phys. Chem. B* **114**, 15445 (2010).
- <sup>10</sup>A. Arbe, J. A. Pomposo, A. J. Moreno, F. LoVerso, M. González-Burgos, I. Asenjo-Sanz, A. Iturrospe, A. Radulescu, O. Ivanova, and J. Colmenero, *Polymer* **105**, 532 (2016).
- <sup>11</sup>M. A. Calabrese and N. J. Wagner, *ACS Macro Lett.* **7**, 614 (2018).
- <sup>12</sup>M. E. O’Kane, J. A. Smith, R. C. Kilbride, E. L. Spooner, C. P. Duif, T. E. Catley, A. L. Washington, S. M. King, S. R. Parnell, and A. J. Parnell, *Chem. Mater.* **34**, 7232 (2022).
- <sup>13</sup>L. Misuraca, A. Caliò, J. G. LoRicco, I. Hoffmann, R. Winter, B. Demé, J. Peters, and P. M. Oger, *Life* **12**, 445 (2022).
- <sup>14</sup>Y. Liu, *Curr. Opin. Colloid Interface Sci.* **42**, 147 (2019).
- <sup>15</sup>J. S. Gardner, G. Ehlers, A. Faraone, and V. García Sakai, *Nat. Rev. Phys.* **2**, 103 (2020).
- <sup>16</sup>L. Balacescu, T. E. Schrader, A. Radulescu, P. Zolnierczuk, O. Holderer, S. Pasini, J. Fitter, and A. M. Stadler, *Sci. Rep.* **10**, 1570 (2020).
- <sup>17</sup>T. Nawroth, P. Buch, K. Buch, P. Langguth, and R. Schweins, *Mol. Pharmaceutics* **8**, 2162 (2011).
- <sup>18</sup>A. J. Schmid, L. Wiehemeier, S. Jaksch, H. Schneider, A. Hiess, T. Bögershausen, T. Widmann, J. Reitenbach, L. P. Kreuzer, M. Kühnhammer *et al.*, *Appl. Sci.* **11**, 4089 (2021).
- <sup>19</sup>L. Balacescu, G. Brandl, F. Kaneko, T. E. Schrader, and A. Radulescu, *Appl. Sci.* **11**, 5135 (2021).
- <sup>20</sup>L. Balacescu, F. Vögl, S. Staringer, V. Ossovyi, G. Brandl, N. Lumma, H. Feilbach, O. Holderer, S. Pasini, A. Stadler *et al.*, *J. Surf. Invest.: X-Ray, Synchrotron Neutron Tech.* **14**, S185 (2020).
- <sup>21</sup>S. Pasini, O. Holderer, T. Kozielski, D. Richter, and M. Monkenbusch, *Rev. Sci. Instrum.* **90**, 043107 (2019).
- <sup>22</sup>B. Chu, *Laser Light Scattering: Basic Principles and Practice* (Academic Press, 1991).
- <sup>23</sup>D. Arzenšek, R. Podgornik, and D. Kuzman, *Dynamic Light Scattering and Application to Proteins in Solutions* (Department of Physics, University of Ljubljana, 2010), pp. 1–18.
- <sup>24</sup>S. W. Provencher, *Comput. Phys. Commun.* **27**, 229 (1982).
- <sup>25</sup>S. Kalinin, R. Kühnemuth, H. Vardanyan, and C. A. M. Seidel, *Rev. Sci. Instrum.* **83**, 096105 (2012).
- <sup>26</sup>C. Cho, J. Urquidí, S. Singh, and G. W. Robinson, *J. Phys. Chem. B* **103**, 1991 (1999).
- <sup>27</sup>S. Kedenburg, M. Vieweg, T. Gissibl, and H. Giessen, *Opt. Mater. Express* **2**, 1588 (2012).
- <sup>28</sup>K. Kang and K. Sadakane, *J. Phys. Commun.* **5**, 035003 (2021).
- <sup>29</sup>W. Van Meegen and S. M. Underwood, *Phys. Rev. E* **47**, 248 (1993).